Letter

Prediction of high-T_c superconductivity in H_6SX (X = Cl, Br) at pressures below one megabar

Yu-Long Hai,[1] Hui-Li Tian,[1,2] Meng-Jing Jiang,[1,2] Han-Bin Ding,[1,2] Yu-Jie Feng,[1,2] Guo-Hua Zhong,[1,3,*] Chun-Lei Yang,[1,3,†] Xiao-Jia Chen,[4,5,‡] and Hai-Qing Lin[6,§]

[1]*Shenzhen Institute of Advanced Technology, Chinese Academy of Sciences, Shenzhen 518055, China*
[2]*Nano Science and Technology Institute, University of Science and Technology of China, Suzhou 215123, China*
[3]*University of Chinese Academy of Sciences, Beijing 100049, China*
[4]*School of Science, Harbin Institute of Technology, Shenzhen 518055, China*
[5]*Center for High Pressure Science and Technology Advanced Research, Shanghai 201203, China*
[6]*Beijing Computational Science Research Center, Beijing 100193, China*

(Received 14 December 2021; revised 12 May 2022; accepted 19 May 2022; published 31 May 2022)

After the discovery of near room-temperature superconductivity in superhydrides at extremely high pressure close to 300 GPa, there is increasing interest in finding superconducting systems to maintain the similar superconductivity but at pressures below megabar. To examine such a possibility in metal-free hydrides, we investigate the thermodynamical stability and dynamical stability, electronic structures, and electron-phonon interactions of H_6SX (X = Cl and Br) from the theoretical viewpoint. The results show that H_6SCl and H_6SBr are potential superconductors with the transition temperatures of 155.4 K at 90 GPa and 136 K at 140 GPa, respectively. Remarkably, H_6SCl can be stabilized at the pressure above 82.5 GPa but maintain the superconducting transition above 150 K. Compared with H_3S, the substitution of S by Cl with lower electronic energy states leads to the enhancement of Cl-H covalent bonding. As a result, the stable pressure of H_3S-like superconductors is substantially reduced below 100 GPa but the transition temperature can be maintained as high as 150 K.

DOI: 10.1103/PhysRevB.105.L180508

Superconductivity is among the most fascinating phenomena in condensed matter physics. Recently, superconductivity near room temperature was reported in sulfur hydride [1], lanthanum hydride [2,3], and carbonaceous sulfur hydride [4] at high pressures. These superconducting hydrides can only be stabilized at high pressures above 150 GPa. Such a pressure is too high to be achieved in most laboratories, which limits the practical applications. Exploring superconductivity in hydrides at low pressures below 100 GPa becomes the key activity of current research. As the first system with superconductivity of more than 200 K observed, sulfur hydride has been paid much attention. Along with the theoretical prediction of the structure and superconductivity of H_2S [5] and $(H_2S)_2H_2$ [6] under high pressure, researchers have systematically studied the possible structures of the superconducting sulfide hydride and the structural phase diagram under pressure. Based on the metadynamics calculations, Majumdar *et al.* predicted that in the pressure range of 100–140 GPa, hydrogen sulfide exhibits the superconductivity of 80 K in the chemical ratio of H_2S, while above 140 GPa, the phase becomes the chemical ratio of H_3S, showing the superconductivity of 220 K at about 200 GPa [7,8]. The experimental phase diagram of temperature-pressure also shows that the hydrogen sulfide exists in the form of covalent H_3S at low temperature and above 135 GPa [9]. This implies that pure $Im3m$-H_3S suggested by Duan *et al.* [6] is difficult to exist stably at low pressure and will exhibit high-temperature superconductivity. Some new technologies are needed to realize low-pressure and high-T_c superconductivity in H_3S.

Replacing S with elements of the same group, the superconducting phases of H_3Se and H_4Te were found to have the critical temperature T_c of 110–120 K at the pressure of about 100–120 GPa [10,11] and 104 K at 170 GPa [12], respectively. There is no obvious improvement for either increasing T_c or lowering pressure for H_3S upon the substitution of P for S [13,14]. If we substitute P for part S [15], $H_3S_{0.925}P_{0.075}$ and $H_3S_{0.9}P_{0.1}$ can only be stabilized above 150 GPa, although T_c of $H_3S_{0.925}P_{0.075}$ increases from 241 K at 150 GPa to 280 K at 250 GPa. By increasing the doping ratio of P, $H_3S_{0.875}P_{0.125}$ is stable above 100 GPa [16] or dynamically stable in the pressure region of 200–250 GPa with T_c of 215 K at 200 GPa [17]. H_6SP with higher P content can be stabilized at 200 GPa with T_c of about 160 K [18]. Meanwhile, partial substitution for S by Se seemingly does not reduce the pressure for holding high T_c. For example, half substitution of S by Se in H_3S leads to the formation of three phases of $Pm\bar{3}m$, $Cmmm$, and $Fd\bar{3}m$ at 200 GPa with T_c values in the range of 115–196 K [19]. H_6SSe with $Im\bar{3}m$ space group can be superconducting with $T_c \approx$ 182 K at 200 GPa [18]. $H_3S_{0.25}Se_{0.75}$ and $H_3S_{0.75}Se_{0.25}$ are stabilized at 200 GPa or lower pressures but have the T_c values of less than 100 K [20]. The situation remains unchanged even for carbonaceous sulfur hydrides [4,21–23]. The metastable CSH_7 was suggested to be a superconductor with T_c ranging from 100 to 190 K in the pressure range of 100–250 GPa

*gh.zhong@siat.ac.cn
†cl.yang@siat.ac.cn
‡xjchen@hpstar.ac.cn
§haiqing0@csrc.ac.cn

[21]. When the content of C in H_3S is decreased, the calculation based on virtual crystal approximation brings about T_c exceeding 200 K at 250 GPa or higher pressures [22], while the calculation starting from supercell indicates that it is difficult for H_3S with dilute carbon to achieve high-temperature superconductivity below 100 GPa [23]. Interestingly, doping halogen elements in the H-S system was reported to lower the pressure for the stable superconducting phase such as H_6SBr with T_c of 174 K at 150 GPa [18]. While the trend for the T_c evolution with pressure in such a family is still unclear, one always hopes to maintain high-T_c superconductivity in these materials at pressures as low as possible. Noticeably, the dynamical stability of Cl doped H_3S can be extrapolated to 140 GPa [16]. There is no clue for the T_c behavior of H_3S with higher Cl content. The Br-doped case also deserves further study.

To address the above mentioned issues, selecting Cl and Br with similar radius to S atom, we study the doping effect in H_3S with Cl and Br substitutions based on the first-principles calculations. The thermodynamics and molecular dynamics including pressure and temperature effects are used to analyze the stability of materials. The superconductivity with relatively high T_c values is predicted for these hydrides at expected easily accessible low pressures. The synthesized conditions of pressure and temperature for those superconductors are given.

The structural predictions of H_6SX (X = Cl and Br) at different pressures were performed by the swarm intelligence-based CALYPSO method [24–26]. The calculations of structural optimization and electronic structures were carried out by employing the Vienna ab initio simulation package (VASP) [27,28] within the framework of the density functional theory based on the Perdew-Burke-Ernzerhof (PBE) generalized gradient approximation (GGA) [29] and the projector augmented wave pseudopotential [30]. The plane-wave cut-off energy was set as 600 eV. The k point of the Brillouin zone was 0.02 $Å^{-1}$ interval distribution of Monkhorst-Pack for the optimization of structures, and the k-point interval of the total energy self-consistent calculation was 0.01 $Å^{-1}$ or better. Convergence thresholds were set as 10^{-5} eV in energy and 10^{-3} eV/Å in force. In addition, based on a $4 \times 4 \times 4$ supercell containing 512 atoms, we adopted Car and Perriello molecular dynamics [31] and NVT ensemble to examine the stability of H_6SCl and H_6SBr at constant temperature and pressure. Nosé-Hoover thermostat [32] was used to ensure that the ambient temperature is controlled at the set value.

With the help of density functional perturbation theory and PBE-GGA functional, QUANTUM ESPRESSO package (QE) [33,34] was used to calculate the phonon frequency (ω) and the Eliashberg electron-phonon spectral function [$\alpha^2F(\omega)$]. Based on $\alpha^2F(\omega)$, the electron-phonon coupling constant (λ, EPC) was calculated, which is defined by integration over the entire frequency domain of $\alpha^2F(\omega)$:

$$\lambda = 2\int_0^\infty \frac{\alpha^2F(\omega)}{\omega}d\omega. \tag{1}$$

For $\lambda < 1.5$, T_c was estimated by the McMillan equation [35], expressed as

$$T_c = \frac{\omega_{\log}}{1.2}\exp\left[-\frac{1.04(1+\lambda)}{\lambda-\mu^*(1+0.62\lambda)}\right]. \tag{2}$$

The EPC parameter λ is larger than 1.5, which represents very strong electron-phonon coupling for systems. T_c was corrected by the Allen-Dynes-corrected McMillan equation [36], expressed as

$$T_c = f_1 f_2 \frac{\omega_{\log}}{1.2}\exp\left[-\frac{1.04(1+\lambda)}{\lambda-\mu^*(1+0.62\lambda)}\right], \tag{3}$$

where

$$f_1 = \left\{1+\left[\frac{\lambda}{2.46(1+3.8\mu^*)}\right]^{3/2}\right\}^{1/3}, \tag{4}$$

$$f_2 = 1+\frac{\lambda^2(\omega_2/\omega_{ln}-1)}{\lambda^2+[1.82(1+6.3\mu^*)(\omega_2/\omega_{ln})]^2} \tag{5}$$

are the correction factors. $\omega_{\log}$ is the logarithmic average of phonon frequency and is written as

$$\omega_{\log} = \exp\left[\frac{2}{\lambda}\int_0^\infty \frac{\alpha^2F(\omega)\log(\omega)}{\omega}d\omega)\right]. \tag{6}$$

The typical value of Coulomb pseudopotential μ^* was set as 0.1 for hydrides. Vanderbilt-type ultrasoft pseudopotentials were formulated for the PBE functional in this calculation [37]. A k mesh of $16 \times 16 \times 16$ in the first Brillouin zone was used in the calculation of the electron-phonon interaction matrix element and a q mesh of $4 \times 4 \times 4$ was used for the phonon spectra calculation. The cut-off energies for wave function and charge density were set as 80 and 600 Ry, respectively. At the same time, the force and stress of the convergent structure were optimized and controlled within the error range of VASP and QE programs.

Our results show that H_6SCl possesses relatively high T_c at low pressure. In the following discussion, H_6SCl is thus taken as an example to illustrate the stability, electronic properties, and possible superconductivity. The results of H_6SBr are presented in the Supplemental Material [38]. By substituting Cl or Br for half of the S atoms in H_3S structure, as shown in Fig. S1 [38], the doped structure has the symmetry of $Pm\bar{3}m$ instead of $Im\bar{3}m$. H_6SCl has many similar properties to the parent H_3S in the structure. For example, it is a body-centered cubic (bcc) structure, and the position of each face center of the unit cell is occupied by H atom. But the difference is that the position of the body center is occupied by Cl atom. Therefore, due to the subtle structural difference, we also reexamined the thermodynamic stability of H_6SCl. The possible phase transitions induced by pressure were first investigated. Figure 1 shows the change of enthalpy for relatively stable phases of H_6SCl with pressure. (All structure files are presented in the Supplemental Material [38].) The zero-point energy effect has also been taken into account in the calculation of enthalpies at different pressures. From the results of enthalpy versus pressure, we can find that H_6SCl has five structural transitions in the range of 0–200 GPa. Below 7 GPa, H_6SCl is stabilized at $P\bar{1}$ phase, next it transforms into $Cmm2$ phase in $7-39$ GPa, then it becomes a $Cm2m$ structure in 39–60 GPa, and then it transforms into $C2$ phase in 60–85 GPa, after that it exits in the form of $Pm\bar{3}m$ phase in 85–195 GPa, and finally it is stabilized at $R3$ phase above 195 GPa.

Furthermore, the enthalpy of formation of H_6SCl is compared with several possible decomposition enthalpies. As

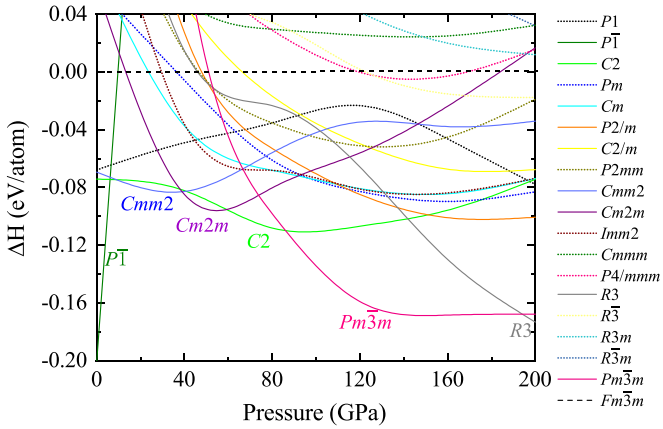

FIG. 1. The pressure as function of relative enthalpies for competitive structures of H_6SCl to the $Fm\bar{3}m$ phase.

shown in Fig. 2, when the enthalpy of formation of $1/2(2HCl + 2H_2S + 3H_2)$ is used as the reference, the enthalpy of H_6SCl, $H_3Cl + H_3S$, and $Cl + S + 3H_2$ is significantly lower than that of $1/2(2HCl + 2H_2S + 3H_2)$ in the pressure range of 0–200 GPa. Noticeably, H_6SCl is only thermodynamically stable above 82.5 GPa, while below this pressure, it is unstable and possibly decomposed into $Cl + S + 3H_2$. However, the stable pressure range of doped H_3S has been extended to lower pressures, such as 82.5 GPa, which is already below the megabar pressure level. Combining the phase transitions ordering shown in Fig. 1 with the enthalpy of formation shown in Fig. 2, we conclude that H_6SCl can stably exist in the pressure range 85–195 GPa in the form of $Pm\bar{3}m$ structure. These two phases of $C2$ and $R3$ are ignored since they are only stable in a narrow pressure region of 82.5–85 GPa for $C2$ and 195–200 GPa for $R3$, respectively.

The structural stability of H_6SCl was also analyzed under the combined action of pressure and temperature from the perspective of molecular dynamics. When H_6SCl was applied

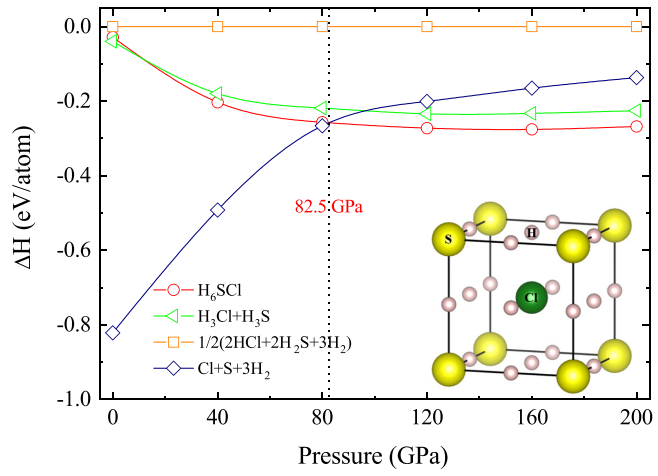

FIG. 2. Enthalpy difference vs pressure for H_6SCl, referenced to the decomposition enthalpy into $1/2(2HCl + 2H_2S + 3H_2)$. The decomposition enthalpies into $H_3Cl + H_3S$ and $Cl + S + 3H_2$ were also plotted, respectively. Inset is the crystal structure of H_6SCl in the form of a unit cell.

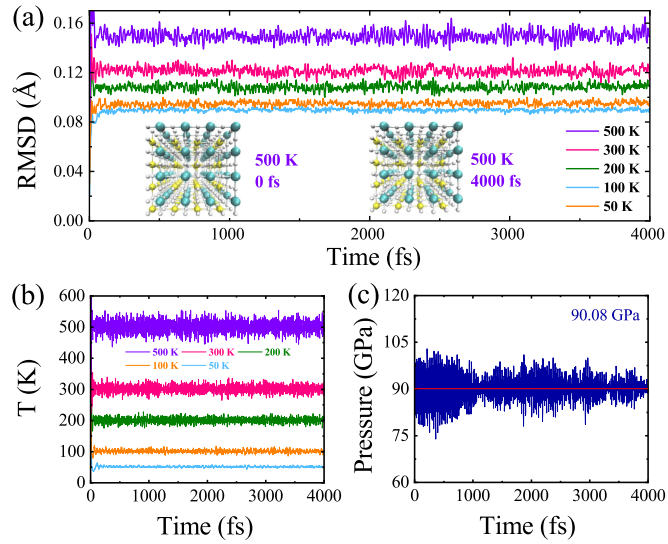

FIG. 3. (a) RMSD of H_6SCl in the temperature range of 50–500 K at 90 GPa. Inset shows two $4 \times 4 \times 4$ supercell structures corresponding to 0 and 4000 fs, respectively. (b) Thermostat temperature oscillation in the range of 50–500 K. (c) Pressure oscillation at 90 GPa.

with pressure of 90 GPa, the molecular dynamics were simulated at the temperature of 50, 100, 200, 300, and 500 K. The relaxation process at different temperatures is shown in Fig. 3(a). The root-mean-square displacements (RMSD) of H_6SCl at 50, 100, 200, 300, and 500 K are 0.089, 0.094, 0.108, 0.121, and 0.149 Å, respectively. For temperature control, we set the temperature of the thermostat to 50, 100, 200, 300, and 500 K, and the actual temperature of the thermostat was fluctuated near the set value, as shown in Fig. 3(b). By averaging the temperature of 0–4000 fs, the average values of the actual temperature are 51.69, 101.49, 200.66, 301.58, and 500.58 K, respectively. Similarly, as shown in Fig. 3(c), when the simulated pressure is 90 GPa, the actual pressure is 90.08 GPa. Therefore, at the pressure of 90 GPa, when we apply the temperature of 50–500 K to H_6SCl, it can still maintain the stability and integrity of the structure. When the pressure rises to 200 GPa, the atomic RMSD and temperature oscillation in the temperature range of 50–500 K as well as the pressure oscillation is similar to those at 90 GPa, as shown in Figs. S2– S4 [38]. Therefore, H_6SCl still maintains dynamical stability under certain conditions. It is clear that H_6SCl can still keep the stability of the structure after considering the influence of certain temperature. Namely, H_6SCl is thermodynamically and dynamical stable in the pressure range of 85–200 GPa.

After confirming the stability of H_6SCl, the electronic structures were investigated. Figure 4(a) shows the electron localization function (ELF) on (002) and (001) planes of H_6SCl at 90 GPa. There are only Cl and H atoms on (002) plane, while there are only S and H atoms on the (001) plane. From the ELF, it is found that there is stronger covalent bond between Cl and H than between S and H, which is because Cl has stronger electronegativity than S and the atomic radius close to S [39]. The stronger covalent bond results in the stability of H_6SCl at lower pressure. Similar to H_3S, there is

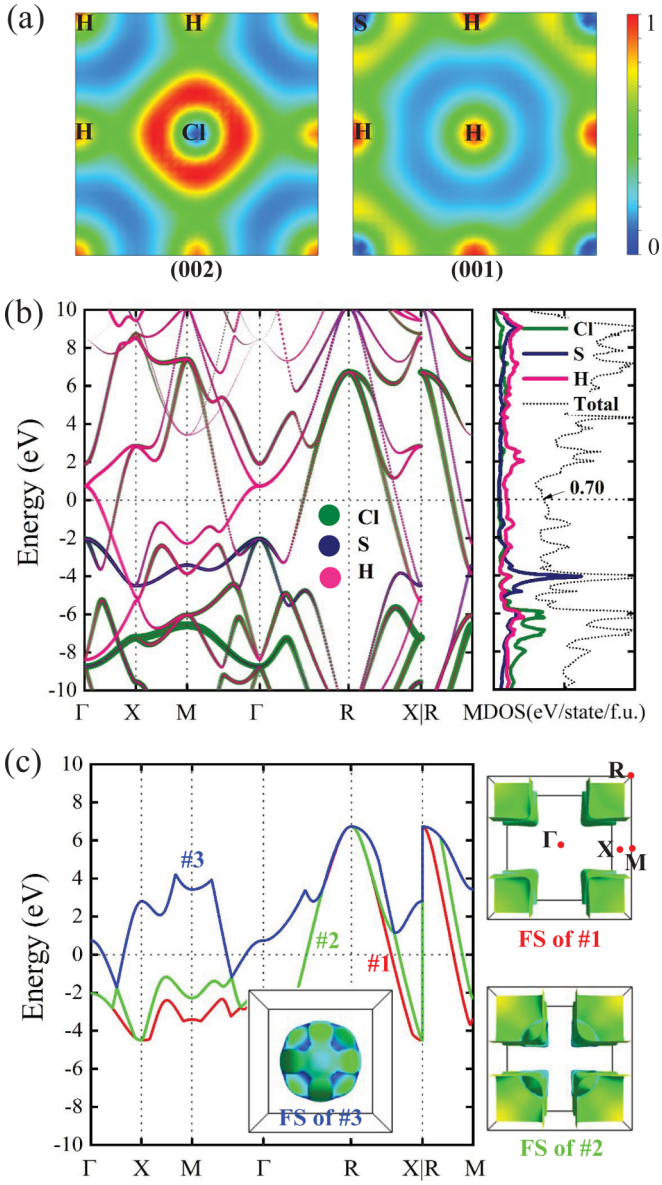

FIG. 4. Calculated ELF on (002) and (001) planes (a), projected band structure and DOS on each element (b), and Fermi surface sheets corresponding to energy bands crossing the Fermi level (c) for H_6SCl at 90 GPa.

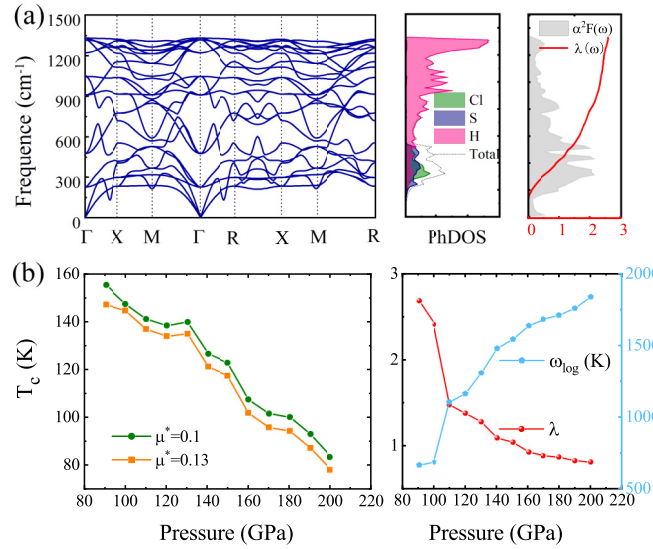

FIG. 5. (a) Phonon spectrum, phonon density of states (PhDOS), and Eliashberg spectrum function $\alpha^2F(\omega)$, and electron-phonon coupling integral $\lambda(\omega)$ of H_6SCl at 90 GPa. (b) Pressure dependence of T_c, λ, and ω_{log} of H_6SCl.

no covalent bond between two H atoms in H_6SCl. The energy band structure of H_6SCl at 90 GPa was calculated along high symmetrical k-point paths of $\Gamma - X - M - \Gamma - R - X$ and $R - M$ in reciprocal space of $Pm\bar{3}m$. As shown in Fig. 4(b), H_6SCl exhibits the metallic electronic characteristics under pressure. The contribution of each element to the energy band was distinguished by different colors in Fig. 4(b). Combining with the projected density of states (DOS) on element, we can observe that the contribution of H to the electronic states near the Fermi level is larger than those of Cl and S. Unlike the visible van Hove singularity at the Fermi level in H_3S [6,40], it is reduced in H_6SCl. However, the total DOS value at the Fermi level is 0.70 eV/state/f.u. at 90 GPa, which is larger than 0.45 eV/state/f.u. of H_3S at 200 GPa [6]. As the pressure is increased, the total DOS value at the Fermi level is only slightly decreased (Fig. S5 [38]). From the fine electronic structures, Cl-dominated bands (states) have lower energy than S-dominated bands (states), which is consistent with the existence of stronger bonding states between Cl and H. Three energy bands crossing the Fermi level are demonstrated separately in Fig. 4(c). Each band is formed by the mixing of Cl, S, and H electronic states. Bands 1 and 2 have the large degeneracy in the $\Gamma - R - X$ direction. They thus form the similar Fermi surface (FS) sheets including electron-like and hole-like features. Band 3 forms the electron-like FS sheets along the $\Gamma - X$ and $M - \Gamma$ directions. From the 2D projection of FS (Fig. S7 [38]), visible nesting characteristics of FS are observed in H_6SCl. The existence of nesting phenomenon implies the occurrence of superconducting phase transition.

Before evaluating superconductivity, the phonon band structures of H_6SCl were calculated. The evolution of phonon spectra with pressure is shown in the Fig. S8 [38], which again implies the dynamical stability of H_6SCl at high pressure. Figure 5(a) shows the phonon spectra, phonon density of states (PhDOS), Eliashberg spectrum function $\alpha^2F(\omega)$, and electron-phonon coupling integral $\lambda(\omega)$ of H_6SCl at 90 GPa, respectively. As can be seen, the frequency range of the phonon vibration of H_6SCl is 0–1350 cm^{-1}. Among them, some parts of the high-frequency modes come from the vibration of H atoms, while the low-frequency phonon in the region of 0–600 cm^{-1} is mainly due to the vibrations of Cl and S, although H also participates in part of the low-frequency vibration. A large number of soft phonon modes can be observed from the phonon spectra, which is from the shielding effect of electrons on lattice vibrations. The Kohn anomalies imply the strong electron-phonon coupling interactions in H_6SCl. By integrating the Eliashberg function, we can obtain the EPC constant λ. In the low-frequency part, the growth rate of λ is very fast, that is, the vibration of Cl and S in the low-frequency part makes a large contribution

to the EPC. Increasing the frequency, the vibrations of Cl and S gradually disappear, and H element dominates in the high frequency part. As shown in Fig. 5(b) and Table S1 [38], the total EPC constant reaches 2.69 at 90 GPa, which is larger than 2.19 of H_3S at 200 GPa [6]. However, because $\omega_{\log}$ is only 667.80 K (1334.6 K for H_3S at 200 GPa) at low pressure, the T_c of H_6SCl is predicted as 155.4 K for $\mu^* = 0.1$, which is lower than 204 K of H_3S at 200 GPa [6]. Comparing with H_3S, the smaller $\omega_{\log}$ mainly comes from the increase of lattice constant after doping. The lattice constant of $a = 3.203$ Å at 90 GPa for H_6SCl is larger than 2.984 Å of H_3S at 200 GPa [6]. The volume expansion at low pressure results in the decrease of phonon frequency. As a result, H_6SCl at 90 GPa has smaller $\omega_{\log}$ than H_3S at 200 GPa. Compared with $H_3S_{0.9375}Cl_{0.0625}$ and $H_3S_{0.875}Cl_{0.125}$ [16,17], H_6SCl with the high doping content of Cl substantially reduces the stable pressure while maintaining high T_c. Figure 5(b) displays the pressure dependence of T_c, λ, and $\omega_{\log}$ of H_6SCl. T_c rapidly decreases with increasing pressure. When increasing pressure to 200 GPa, T_c is reduced to 83.4 K for $\mu^* = 0.1$. The EPC constant λ has a similar trend with pressure, while $\omega_{\log}$ behaves in an opposite way. Therefore, T_c is controlled by the competition between λ and $\omega_{\log}$. As a result, the substitution of Cl for half of S in H_3 drops the stable pressure below 100 GPa while keeping high T_c above 150 K.

For the Br-doped case, the electronic structures shown in Fig. S6 [38] shows its metallization at high pressure. The phonon spectra shown in Fig. S9 [38] and the RMSD shown in Fig. S10 [38] indicate that H_6SBr is dynamically stable above 120 GPa. The predicted T_c of H_6SBr is 125.12 K at 120 GPa, and T_c first increases and then decreases with the increase of pressure, as shown in Table S1 [38]. However, compared with H_6SCl, H_6SBr cannot be stabilized at lower pressures such as below 100 GPa.

In summary, we have studied the structural stability (thermodynamic and dynamical stabilities), electronic structures, phonon characteristics, and electron-phonon interactions in H_3S through the substitution of halogen elements (Cl and Br) for S under pressure based on the first-principles calculations. We found that among the substituted systems, H_6SCl and H_6SBr exhibit the structural stability and superconductivity with the transition temperatures of 155.4 and 136.4 K at pressures of 90 and 140 GPa, respectively. The discovery of H_6SCl is significant for the exploration of low-pressure and high-temperature superconductivity. H_6SCl can be stabilized at the pressure around 85 GPa in form of $Pm\bar{3}m$. The stable pressure of H_3S-like superconductors is reduced below 100 GPa at which superconductivity can be maintained as high as 150 K.

The work was supported by the National Natural Science Foundation of China (Grant No. 12074401), the Shenzhen Science and Technology Program (Grants No. JCYJ20180507182445460, No. JCYJ20200109112810241, and No. KQTD20200820113045081), and the National Key R&D Program of China (Grant No. 2018YFA0305900). This work was also supported by the SIAT-CUHK Joint Laboratory of Photovoltaic Solar Energy. The calculations were performed in HPC Laboratory, National Supercomputing Center in Shenzhen and the Beijing Computational Science Research Center, respectively.

[1] A. P. Drozdov, M. I. Eremets, I. A. Troyan, V. Ksenofontov, and S. I. Shylin, Nature (London) **525**, 73 (2015).
[2] A. P. Drozdov, P. P. Kong, V. S. Minkov, S. P. Besedin, M. A. Kuzovnikov, S. Mozaffari, L. Balicas, F. F. Balakirev, D. E. Graf, V. B. Prakapenka *et al.*, Nature (London) **569**, 528 (2019).
[3] M. Somayazulu, M. Ahart, A. K. Mishra, Z. M. Geballe, M. Baldini, Y. Meng, V. V. Struzhkin, and R. J. Hemley, Phys. Rev. Lett. **122**, 027001 (2019).
[4] E. Snider, N. Dasenbrock-Gammon, R. McBride, M. Debessai, H. Vindana, K. Vencatasamy, K. V. Lawler, A. Salamat, and R. P. Dias, Nature (London) **586**, 373 (2020).
[5] Y. Li, J. Hao, H. Liu, Y. Li, and Y. Ma, J. Chem. Phys. **140**, 174712 (2014).
[6] D. Duan, Y. Liu, F. Tian, D. Li, X. Huang, Z. Zhao, H. Yu, B. Liu, W. Tian, and T. Cui, Sci. Rep. **4**, 6968 (2015).
[7] A. Majumdar, J. S. Tse, and Y. Yao, Angew. Chem. Int. Ed. **56**, 11390 (2017).
[8] A. Majumdar, J. S. Tse, and Y. Yao, Sci. Rep. **9**, 5023 (2019).
[9] E. J. Pace, X.-D. Liu, P. Dalladay-Simpson, J. Binns, M. Peña-Alvarez, J. P. Attfield, R. T. Howie, and E. Gregoryanz, Phys. Rev. B **101**, 174511 (2020).
[10] S. Zhang, Y. Wang, J. Zhang, H. Liu, X. Zhong, H.-F. Song, G. Yang, L. Zhang, and Y. Ma, Sci. Rep. **5**, 15433 (2015).
[11] J. A. Flores-Livas, A. Sannaa, and E. K. U. Gross, Eur. Phys. J. B **89**, 63 (2016).
[12] X. Zhong, H. Wang, J. Zhang, H. Liu, S. Zhang, H.-F. Song, G. Yang, L. Zhang, and Y. Ma, Phys. Rev. Lett. **116**, 057002 (2016).
[13] T. Bi, D. P. Miller, A. Shamp, and E. Zurek, Angew. Chem. **129**, 10326 (2017).
[14] Y. Yuan, Y. Li, G. Fang, G. Liu, C. Pei, X. Li, H. Zheng, K. Yang, and L. Wang, Natl. Sci. Rev. **6**, 524 (2019).
[15] Y. Ge, F. Zhang, and Y. Yao, Phys. Rev. B **93**, 224513 (2016).
[16] A. Nakanishi, T. Ishikawa, and K. Shimizu, J. Phys. Soc. Jpn. **87**, 124711 (2018).
[17] H. Guan, Y. Sun, and H. Liu, Phys. Rev. Research **3**, 043102 (2021).
[18] Z. Shao, H. Song, H. Yu, and D. Duan, J. Supercond. Novel Magn. (2021), doi: 10.1007/s10948-021-06061-z.
[19] B. Liu, W. Cui, J. Shi, L. Zhu, J. Chen, S. Lin, R. Su, J. Ma, K. Yang, M. Xu *et al.*, Phys. Rev. B **98**, 174101 (2018).
[20] M. Amsler, Phys. Rev. B **99**, 060102(R) (2019).
[21] W. Cui, T. Bi, J. Shi, Y. Li, H. Liu, E. Zurek, and R. J. Hemley, Phys. Rev. B **101**, 134504 (2020).
[22] Y. Ge, F. Zhang, R. P. Dias, R. J. Hemley, and Y. Yao, Mater. Today Phys. **15**, 100330 (2020).
[23] X. Wang, T. Bi, K. P. Hilleke, A. Lamichhane, R. J. Hemley, and E. Zurek, npj Comput. Mater. **8**, 87 (2022).
[24] Y. Wang, J. Lv, L. Zhu, and Y. Ma, Phys. Rev. B **82**, 094116 (2010).
[25] Y. Wang, J. Lv, L. Zhu, and Y. Ma, Comput. Phys. Commun. **183**, 2063 (2012).
[26] B. Gao, P. Gao, S. Lu, J. Lv, Y. Wang, and Y. Ma, Sci. Bull. **64**, 301 (2019).
[27] G. Kresse and J. Furthmuller, Comput. Mater. Sci. **6**, 15 (1996).
[28] G. Kresse and J. Furthmuller, Phys. Rev. B **54**, 11169 (1996).

[29] J. P. Perdew, K. Burke, and M. Ernzerhof, Phys. Rev. Lett. **77**, 3865 (1996).
[30] G. Kresse and D. Joubert, Phys. Rev. B **59**, 1758 (1999).
[31] R. Car and M. Parrinello, Phys. Rev. Lett. **55**, 2471 (1985).
[32] W. G. Hoover, Phys. Rev. A **31**, 1695 (1985).
[33] P. Giannozzi, S. Baroni, N. Bonini, M. Calandra, R. Car, C. Cavazzoni, D. Ceresoli, G. L. Chiarotti, M. Cococcioni, I. Dabo *et al.*, J. Phys.: Condens. Matter **21**, 395502 (2009).
[34] P. Giannozzi Jr., O. Andreussi, T. Brumme, O. Bunau, M. B. Nardelli, M. Calandra, R. Car, C. Cavazzoni, D. Ceresoli, M. Cococcioni *et al.*, J. Phys.: Condens. Matter **29**, 465901 (2017).
[35] R. C. Dynes, Solid State Commun. **10**, 615 (1972).
[36] P. B. Allen and R. C. Dynes, Phys. Rev. B **12**, 905 (1975).
[37] D. Vanderbilt, Phys. Rev. B **41**, 7892 (1990).
[38] See Supplemental Material at http://link.aps.org/supplemental/10.1103/PhysRevB.105.L180508 for crystal structural characteristics, molecular dynamics data, electronic structures, phonon spectra, and superconducting parameters of H_6SX (X = Cl and Br) at selected pressures as well as the POSCAR files of H_6SCl at stable pressure.
[39] The Pauling electronegativity of Cl and S is respectively 3.16 and 2.58, and the atomic radii data of S and Cl are both 100 pm at https://www.webelements.com.
[40] Y. Quan and W. E. Pickett, Phys. Rev. B **93**, 104526 (2016).